Published in final edited form as:
J Neurochem. 2007 March ; 100(5): 1397–1406. doi:10.1111/j.1471-4159.2006.04323.x.

Neurochemical changes in Huntington R6/2 mouse striatum detected by *in vivo* ^{1}H NMR spectroscopy

Ivan Tkac[*], **Janet M. Dubinsky**[†], **C. Dirk Keene**[‡,1], **Rolf Gruetter**[*,2], and **Walter C. Low**[§]

[*]Center for Magnetic Resonance Research, University of Minnesota, Minneapolis, Minnesota, USA

[†]Department of Neuroscience, University of Minnesota, Minneapolis, Minnesota, USA

[‡]Graduate Program in Neuroscience, University of Minnesota, Minneapolis, Minnesota, USA

[§]Department of Neurosurgery, University of Minnesota, Minneapolis, Minnesota, USA

Abstract

The neurochemical profile of the striatum of R6/2 Huntington's disease mice was examined at different stages of pathogenesis using *in vivo* ^{1}H NMR spectroscopy at 9.4 T. Between 8 and 12 weeks, R6/2 mice exhibited distinct changes in a set of 17 quantifiable metabolites compared with littermate controls. Concentrations of creatine, glycerophosphorylcholine, glutamine and glutathione increased and *N*-acetylaspartate decreased at 8 weeks. By 12 weeks, concentrations of phosphocreatine, taurine, ascorbate, glutamate, and *myo*-inositol increased and phophorylethanolamine decreased. These metabolic changes probably reflected multiple processes, including compensatory processes to maintain homeostasis, active at different stages in the development of HD. The observed changes in concentrations suggested impairment of neurotransmission, neuronal integrity and energy demand, and increased membrane breakdown, gliosis, and osmotic and oxidative stress. Comparisons between metabolite concentrations from individual animals clearly distinguished HD transgenics from non-diseased littermates and identified possible markers of disease progression. Metabolic changes in R6/2 striata were distinctly different from those observed previously in the quinolinic acid and 3NP models of HD. Longitudinal monitoring of changes in these metabolites may provide quantifiable measures of disease progression and treatment effects in both mouse models of HD and patients.

Keywords

In vivo ^{1}H NMR spectroscopy; quantification; neurochemical profile; Huntington's disease; transgenic mice

Huntington's disease (HD) is characterized initially by selective degeneration of medium spiny GABAergic projection neurons in the neostriatum (Vonsattel *et al*. 1985), and involves progressive motor, cognitive, and psychiatric dysfunction (Huntington 1872; Nance 1998). Huntington's disease is caused by an expansion of the CAG repeat region beyond 37 trinucleotides with age of onset inversely proportional to repeat length (Huntington's Disease

Address correspondence and reprint requests to Janet M. Dubinsky, Ph.D., Department of Neuroscience, University of Minnesota, 6-145 Jackson Hall, 321 Church St. SE, Minneapolis, MN 55455, USA. dubin001@umn.edu.
[1]The present address of C. Dirk Keene is the Department of Pathology, University of Washington, Seattle, WA, USA.
[2]The present address of Rolf Gruetter is the Centre d'Imagerie Biomedicale, Ecole Polytechnique Federale de Lausanne, Lausanne, Switzerland.

Collaborative Research Group. 1993; Duyao *et al*. 1993). The precise mechanism of HD pathophysiology is unknown, although substantial evidence exists for multiple degenerative pathways, including mitochondrial impairment, oxidative stress, caspase activation and apoptosis, impaired gene transcription, and altered protein activity and interactions (Landles and Bates 2004; Li and Li 2004; Beal 2005). Critical insights into the pathophysiology of HD can be derived from direct longitudinal studies of the CNS in pre-symptomatic and affected HD patients (Rosenblatt *et al*. 2003; Aylward *et al*. 2004). However, because of the inherent difficulties in accessing human CNS tissue, biochemical studies of HD have been performed on postmortem specimens, non-CNS tissues, such as lymphoblasts or muscle, or extracellular sources, such as serum or cerebrospinal fluid (Dunlop *et al*. 1992; Nicoli *et al*. 1993; Sawa *et al*. 1999; Lodi *et al*. 2000; Garseth *et al*. 2000).

In vivo ^{1}H nuclear magnetic resonance (NMR) spectroscopy is a unique method for non-invasive quantification of tissue metabolites. It has been used to examine neurochemical changes in multiple neurological disorders, including epilepsy, brain tumors, multiple sclerosis, stroke, and Parkinson's and Alzheimer's disease (Bonavita *et al*. 1999). Previous ^{1}H NMR spectroscopic studies in HD patients have reported changes in signal intensity ratios of four brain metabolites: *N*-acetylaspartate (NAA), total creatine (tCr), choline-containing compounds (Cho), and lactate (Jenkins *et al*. 1993; Koroshetz *et al*. 1997; Harms *et al*. 1997; Jenkins *et al*. 1998). In majority of studies, the tCr signal was used as an internal reference. However, reported changes in tCr levels (Sanchez-Pernaute *et al*. 1999) make interpretation of such ratios difficult.

Development of a number of mouse models of HD have provided rich resources for studying disease progression (Levine *et al*. 2004). Long echo-time *in vivo* ^{1}H NMR spectroscopy has been used to monitor the decrease of NAA/tCr signal ratio during disease progression in several different genetic mouse models of HD (Jenkins *et al*. 2000; van Dellen *et al*. 2000; Jenkins *et al*. 2005). In addition, changes in signal intensity of Cho, taurine (Tau), and the sum of glutamine and glutamate (Glx) relative to tCr were reported for 12-week-old R6/2 and N171-82Q HD mice (Jenkins *et al*. 2005). *In vitro* ^{1}H NMR spectroscopy of brain tissue extracts (Jenkins *et al*. 2000) and magic angle spinning ^{1}H NMR spectroscopy of *ex vivo* brain samples (Tsang *et al*. 2006) were used to study neurochemical changes in multiple brain metabolites.

Recent technical and methodological developments in high-field *in vivo* NMR spectroscopy have dramatically increased the neurochemical information content achievable from *in vivo* ^{1}H NMR spectra. Concentrations of up to 18 brain metabolites (termed a neurochemical profile) can be reliably quantified from the ultra-short echo-time ^{1}H NMR spectra acquired at 9.4 T (Pfeuffer *et al*. 1999; Tkac *et al*. 2003, 2004). This approach was used to reveal alterations in the neurochemical profile of quinolinic acid-lesioned rat striatum (Tkac *et al*. 2001). However, this acute excitotoxic model of HD cannot address specific mechanisms of polyglutamine pathophysiology. Therefore, we decided to study a well established genetic model of HD using high performance *in vivo* ^{1}H NMR spectroscopy at 9.4 T. The aim of the present study was to characterize the neurochemical profile of the striatum of R6/2 mice (Mangiarini *et al*. 1996) and monitor its changes at two time points during disease progression.

Methods

R6/2 Mice

Animal breeding and experiments were performed according to procedures approved by the University of Minnesota Institutional Animal Care and Use Committee. R6/2 founders were purchased from the Jackson Laboratories (Bar Harbor, ME, USA) and bred by crossing

transgenic males and wild type (WT) females at 5 weeks of age. Offspring were genotyped according to established procedures (Mangiarini *et al*. 1996)and the Jackson Laboratory). In brief, DNA was purified from blood derived from the tail vein of recently weaned mice using standard practices (Gentra). PCR of tail DNA was performed according to protocols provided by the Jackson Laboratory using oligonucleotide primers OIMR494 (CGGCTGAGGCAGCAGCGGCTGT) and OIMR495 (GCAGCAGCAGCAGCAACAGCCGCCACCGCC) (University of Minnesota Microchemical Facility) in AM buffer, 10% DMSO, 200 mmol/L dNTP's, 10 ng/mL primers with 0.5 U/mL Taq polymerase (Boehringer Mannheim, Gaithersburg, MD, USA). Cycling conditions were 90″ @ 94°C, 35 cycles @ (30″ @ 94°C, 30″ @ 65°C, 90″ @ 72°C), 10′ @ 72°C. Reaction products were analyzed on a 3% agarose gel (Bio-Rad, Hercules, CA, USA) run at 150 V for 45 min. Transgene detection was facilitated using 100 bp oligonucleotide ladder (Bio-Rad) and illumination by GelStar (Cambrex Bio Science, Baltimore, MD, USA).

Animal preparation

Anesthesia was induced and maintained by flowing a gas mixture (O_2 : N_2O = 1 : 1) containing 1.5–2.0% of isoflurane through the chamber. For R6/2 mice, isoflurane levels were reduced to 1.25% during the experiment. Spontaneously breathing mice were fixed in a cylindrical chamber and the air temperature surrounding the chamber was maintained at 30°C by warm water circulation. The typical duration of the study for a single animal was approximately 1 h, but never exceeded 90 min. *In vivo* ^{1}H NMR spectra were collected from 8 (n = 7) and 12 (n = 6) week-old R6/2 mice and from 8 (n = 8) and 12 (n = 9) week-old WT littermate controls.

In vivo ^{1}H NMR spectroscopy

All experiments were performed on a 9.4 T/31 cm magnet (Magnex Scientific, Abingdon, UK) equipped with an 11 cm gradient coil insert (300 mT/m, 500 μs) and strong custom-designed second-order shim coils (Magnex Scientific, Abingdon, UK) (Tkac *et al*. 2004). The magnet was interfaced to a Varian INOVA console (Varian, Inc., Palo Alto, CA, USA). A quadrature surface RF coil with two geometrically decoupled single-turn coils (of 14 mm diameter) was used for both RF transmission and reception. All firstand second-order shim terms were automatically adjusted using FASTMAP with EPI readout (Gruetter 1993; Gruetter and Tkac 2000). Ultra-short echo-time STEAM (echo time TE = 2 ms, middle period TM = 20 ms, repetition time TR = 5 s, number of transients NT = 160) combined with outer volume suppression and VAPOR water suppression was used for localization (Tkac *et al*. 1999, 2004). Data were saved as arrays of FIDs (four transients per FID), corrected for the frequency drift, summed, and finally corrected for residual eddy current effects using the reference water signal. The position of the volume of interest (VOI) was selected based on multi-slice RARE images. VOIs were centered in the left striatum at the level of the anterior commissure. The size of the VOI (7–12 μL) was adjusted to fit the anatomical structure of striatum, exclude the lateral ventricle, and to minimize partial volume effects.

Quantification and statistics

In vivo ^{1}H NMR spectra were analyzed using LCModel (Provencher 1993). The unsuppressed water signal measured from the same VOI was used as an internal reference for the quantification, assuming 80% brain water content. The LCModel analysis calculates the best fit to the experimental spectrum as a linear combination of model, solution spectra of brain metabolites. The following 19 metabolites were included in the basis set: alanine (Ala), ascorbate (Asc), aspartate, creatine (Cr), γ-aminobutyric acid (GABA), glucose (Glc), glutamate (Glu), glutamine (Gln), glutathione (GSH), glycerophosphorylcholine (GPC), *myo*-inositol (*myo*-Ins), lactate (Lac), *N*-acetylaspartate (NAA), *N*-acetylaspartylglutamate

(NAAG), phosphocreatine (PCr), phosphorylcholine (PCho), phosphorylethanolamine (PE), *scyllo*-inositol, and taurine (Tau). In addition, the spectrum of fast relaxing macromolecules, experimentally measured in the mouse brain with an inversion recovery experiment using a short repetition time (TR = 2.0 s, inversion time = 0.675 s), was included in the basis set as previously described (Pfeuffer *et al*. 1999; Tkac *et al*. 2004). Most of metabolites were quantified with Cramer-Rao lower bounds (CRLB) of 3–35%, corresponding to estimated errors in metabolite concentrations of 0.3–0.5 μmol/g. Aspartate and *scyllo*-inositol were quantified with CRLB > 35% in more than 50% of cases and therefore were eliminated from further analysis. Also Ala data from 12-week-old R6/2 mice were not used for further evaluation because of high CRLB. Because of the consistent quantification of GPC and PCho with CRLB below 35% from all individual animals, their concentrations were reported separately despite negative correlations between them in the LCModel fitting algorithm ($r = -0.82$).

Two different statistical procedures were applied to identify changes in metabolite levels. Only comparisons identified as significantly different in both tests were reported. Initially, two-tailed *t*-tests were used to compare metabolite concentrations from striata of WT and R6/2 mice of the same age and to compare metabolite concentrations of the same strains measured at 8 and 12 weeks. To correct for multiple comparisons, *p*-value thresholds $p < 0.01$ (*), $p < 0.002$ (**), and $p < 0.0002$ (***) were used to determine the statistical significance. In addition, *p*-values for metabolite changes were ranked and evaluated using a false discovery rate procedure (Benjamini and Hochberg 1995). The false discovery rate was set so that only one of fifty identified metabolite changes might be erroneous ($q = 0.02$). Analysis of the effects of age and genotype on the summed concentrations (Gln + Glu, Cr + PCr, GPC + PCho) and concentration ratios (Glu/Gln, PCr/Cr, GPC/PCho) was performed by two-way analysis of variance followed by *post hoc* tests with Bonferroni correction (two-way ANOVA, Graphpad Prism, 4.01). For these additional post-test comparisons, $p < 0.05$ (*), $p < 0.001$ (**), $p < 0.001$ (***) were considered significant.

Results

In vivo ^{1}H NMR spectra were acquired from striata of R6/2 and WT mice at 8 and 12 weeks of age (Fig. 1). Corresponding MR images were used to position VOIs in left striatum (Fig. 1 insets). The VOI size was adjusted according to brain morphology, taking into account progressive striatal and cortical atrophy and enlarged ventricles of the R6/2 mice. Shimming resulted in water linewidths of 12–14 Hz with concomitant creatine linewidths of 10–12 Hz. Resulting high spectral resolution enabled unambiguous signal assignment. In addition to the commonly resolved signals of NAA, Cr + PCr, and choline-containing compounds (GPC + PCho), resonances of several other brain metabolites, such as Gln, Glu, *myo*-Ins, and Tau were clearly resolved. Changes between the neurochemical profiles of R6/2 and WT mice were evident from visual inspection of corresponding ^{1}H NMR spectra (Fig. 1). At 8 weeks of age, reductions in NAA and increases in GPC + PCho, Gln, and Cr + PCr were apparent in spectra from R6/2 mice compared with WT controls. At 12 weeks of age, these changes were more pronounced and a considerable increase in the Tau signal was observed.

Neurochemical profiles composed of seventeen brain metabolites were reliably quantified using LCModel fitting analysis from each spectrum. To examine metabolite changes associated with HD, neurochemical profiles of R6/2 mice and WT controls measured at 8 and 12 weeks were compared (Fig. 2). At 8 weeks of age, the most striking changes associated with HD were increases in concentrations of Cr (+38%), Gln (+41%), and GPC (+60%) (Fig. 2, Table 1). Also notable was an increase in GSH (+36%) and a decrease in NAA levels (−16%). At 12 weeks of age, concentrations Gln and GPC continued to increase (+113% and +206%, respectively), Cr and GSH remained elevated and NAA decreased

slightly (−22%). Additional concentration changes were observed in six more metabolites: increases in Asc, PCr, Glu, *myo*-Ins, Tau and a decrease in PE (Fig. 2, Table 1). An increase in Tau (36%) was the most noticeable change at 12 weeks (Figs 1 and 2). Ala, readily detected in WT controls, was below the detection threshold in the 12 week old R6/2 mice, suggesting a decrease in Ala concentration.

Significant age-related changes in the neurochemical profile of WT mice were not found (Fig. 2, Table 1). A decrease in Glu concentration should be viewed only as a trend, because it did not pass both the statistical tests (Table 1). In the R6/2 mice, progressive increases in concentration of PCr, Gln, Glu, Tau and GPC were observed at 12 weeks relative to 8-week-old mice. Significant decreases in concentrations of Glc and Lac between 8 and 12 weeks were observed in R6/2 mice (Fig. 2, Table 1).

To facilitate comparison of these data with previously published spectral analyses reporting relative signal intensities of total Cr, choline-containing compounds and combined glutamate and glutamine (Glx), the sums Cr + PCr, GPC + PCho and Gln + Glu and the concentration ratios, PCr/Cr, GPC/PCho and Glu/Gln, were calculated (Fig. 3). Concentration of Cr + PCr was highly elevated in striatum of R6/2 mice at both ages compared with WT controls (Fig. 3a). However, the PCr/Cr ratio (Fig. 3b) changed between 8 and 12 weeks of age in the R6/2 mice, although neither of these differed significantly with respect to WT controls. Concentration of Gln + Glu did not change between R6/2 and WT mice at 8 weeks, but rose significantly at 12 weeks in R6/2 mice (Fig. 3a). At 8 and 12 weeks of age, the Glu/Gln ratio was significantly decreased (by −36% and −0.46%, respectively) in transgenics relative to controls (Fig. 3b). Both sum GPC + PCho and GPC/PCho ratio increased in striatum of R6/2 mice when compared with WT controls, reflecting the progressive increases in GPC (Fig. 2).

To visualize metabolite concentrations quantified from individual mice and to investigate the relationship between them, pairs of metabolites that changed the most were selected for scatter plots (Fig. 4). While all six scatter plots discriminate HD mice from WT controls at both ages, separation between those two groups was most evident for pairs of Gln versus Cr + PCr (Fig. 4c) and NAA versus Cr + PCr (Fig. 4f). In addition, clusters of data from 12 and 8 week-old R6/2 mice were distinguishable in all scatter plots (Figs. 4a–e) except the NAA versus Cr + PCr plot (Fig. 4f). In the R6/2, concentrations of GPC, Gln, PCr and Tau appear to increase progressively with age. Gln concentrations correlated with GPC (Fig. 4a, $r = 0.81$, $p = 0.0008$), PCr (Fig. 4e, $r = 0.84$, $p = 0.0003$) and Tau (not shown, $r = 0.82$, $p = 0.0006$). Variations in metabolite levels of Gln, GPC, PCr, and Tau were greater in the older, more severely effected R6/2 mice, suggesting differences in disease progression among individual animals. Indeed, the data points with the highest values of GPC, Tau, PCr, and second highest Gln value came from the same animal (Fig. 4, upside-down triangle).

Discussion

These data represent the first non-invasive, longitudinal measurements of absolute metabolite concentrations from a specific brain region in a transgenic mouse model of Huntington's disease. Striatal neurochemical profiles of 17 metabolites, were repeatedly measured from the same animals as disease progressed. This set of metabolites was similar to the previously reported *in vitro* studies of R6/2 mice using tissue extracts (Jenkins *et al*. 2000) or tissue samples (Tsang *et al*. 2006). In addition, *in vivo* measurements eliminated undesirable catabolic processes that occur during *ex vivo* sample handling and enabled detection of labile compounds, e.g., PCr. Precise metabolite quantification and high reproducibility resulted in identification of disease progression among individual animals and clearly distinguished HD transgenics from non-diseased littermates. Key

methodological factors enabling precise metabolite quantification included: (i) increased sensitivity and chemical shift dispersion at 9.4 T; (ii) efficient automatic adjustment of magnetic field homogeneity (shimming); (iii) a pulse sequence providing high localization performance; (iv) minimization of T_2 relaxation and J-evolution with ultra-short TE; and (v) LCmodel analysis that included the macromolecule spectrum in the basis set and the water signal as an internal reference. The resulting high-resolution spectra reliably quantified individual metabolites with similar spectral patterns, such as Gln and Glu, PCr and Cr or GPC and PCho.

By comparing striatal neurochemical profiles of HD transgenic and WT mice a pattern of disease-related changes in metabolic homeostasis at different ages became evident. At 8 weeks of age, metabolic changes reflected the mid-course disease phenotype. Increased concentrations of Gln, GPC, and Cr + PCr and decreased NAA and the Glu/Gln ratio clearly discriminated individual HD transgenic R6/2 mice from WT littermate controls. Surprisingly, the characteristic changes in Cr, Cr + PCr, GSH, NAA and Glu/Gln observed at 8 weeks were not further progressive with increasing age. By 12 weeks, as these animals approached the end of life (Mangiarini *et al*. 1996), additional metabolic changes characterized this later disease state. Concentrations of metabolites such as Tau, Lac and Glu only changed late in the animal's lifespan, potentially identifying a more advanced disease state. Concentrations of Gln, GPC and PCr, as well as the ratio GPC/PCho increased progressively with the age of R6/2 mice. Positive correlations between concentrations of Gln and PCr, GPC or Tau suggested a link between observed changes of these metabolites and the progress of the disease in individual HD transgenic mice. Changes observed at 12 weeks in metabolites, such as PCr, Asc, PE and *myo*-Ins, might have begun earlier, but failed to reach significance by our strict statistical criteria. Thus, we have identified metabolic markers that may characterize different stages of disease in this mouse model of HD.

Among individual R6/2 mice, concentrations of Gln correlated with those of GPC, PCr and Tau, suggesting parallel changes of the underlying mechanisms. As the R6/2 mice became older, the metabolite concentration ranges became broader and farther away from normative values. The scatter of points among mice of similar ages may indicate that disease progression was not identical among animals. While we have no independent measures of disease stage in these animals, we suggest that the concentration changes of these metabolites may be useful in monitoring disease progression. A multiparameter approach to follow metabolite changes may prove useful in monitoring disease progression, especially with respect to therapeutic trials. Indeed, characteristic changes in absolute brain metabolite concentrations have been reported for humans with adrenoleukodystrophy examined at 4 T (Oz *et al*. 2005).

A significant increase in Cr + PCr, typically reported as tCr, was observed at both ages. As tCr is typically used in reporting ratios of other metabolites, care must be taken in interpreting this type of data (Jenkins *et al*. 1993; Taylor-Robinson *et al*. 1996; Jenkins *et al*. 1998; Hoang *et al*. 1998; Jenkins *et al*. 2000, 2005). The increased Cr + PCr at 8 week was the result of Cr alone, and not PCr. Considering the homeostatic need to maintain normal PCr levels and the reported decrease of creatine kinase mRNA in R6/2 striatum (Luthi-Carter *et al*. 2002), an up-regulation of Cr may occur. An increase in kinetic parameters for the creatine kinase reaction has been reported in the 3NP model of HD (Kasparova *et al*. 2005). Decreased respiration and ATP production would also contribute to an increased demand for total creatine (Seong *et al*. 2005; Milakovic and Johnson 2005; Puranam *et al*. 2006). A similar compensatory homeostatic response was observed in the increase in the antioxidants, Asc and GSH probably in response to the reported oxidative stress in R6/2 (Tabrizi *et al*. 2000).

At 12 weeks, the pattern of metabolite changes was not simply an exaggeration of those seen at 8 weeks, as might be expected for a single mechanism mediating an increasingly progressive disease. Between 8 and 12 week, PCr levels and PCr/Cr ratio in the R6/2 striatum increased while Cr + PCr remained elevated. As disease phenotype continuously worsens with age in R6/2, as typified by the continuously increasing Gln, Tau and GPC concentrations, the increase in PCr/Cr ratio may represent a decrease in striatal energy demands rather than an improved energetic status or mitochondrial function. Indeed, striatal glucose utilization decreases between 8 and 12 weeks in R6/2 animals (Wang *et al*. 2005). Progressive tissue atrophy, as suggested by the elevated GPC, a marker of membrane breakdown and altered dendritic morphology, neuronal excitability and neurotrans-mission (Nitsch *et al*. 1992; Klapstein *et al*. 2001), may mediate the decreased energy demand. Similarly, PCr increased relative to Cr in chronically hypoxic rats or insulin hypoglycemia, conditions expected to decrease energy consumption (Thurston *et al*. 1977; Raman *et al*. 2005).

Different disease-related processes may be responsible for the changes in Glu and Gln observed at the two time points as well. At 8 weeks, the increased Gln may represent an imbalance in the Glu–Gln cycling through neurons and astrocytes reflecting compromised glutamatergic neurotrans-mission. Indeed, highly significant decreases in Glu/Gln ratio was observed at 8 weeks despite the unchanged sum of Gln and Glu. The increase in Gln steady-state concentration occurred despite the abnormal astrocytic glutamate uptake following down-regulation of glutamate transporters (Lievens *et al*. 2001; Behrens *et al*. 2002). The source of the increased Gln was not readily apparent, as both glutamine synthase and phosphate activated glutaminase activities are decreased in R6/2 (Butterworth *et al*. 1985; Lievens *et al*. 2001). Net Gln synthesis could not account for the continuous Gln increase, as the sum, Glu + Gln, was not increased at this time. While the excess polyglutamines incorporated in the Huntingtin protein or protein fragments would not be expected to contribute to the ^{1}H NMR signal, an increase in soluble glutamine monomers as a consequence of Huntington degradation remains a remote possibility. At 12 weeks, Gln + Glu increased significantly. Astrocyte proliferation accompanies HD and could account for the increased Gln and *myo*-Ins, which are predominantly found in astrocytes (Norenberg and Martinez-Hernandez 1979; Brand *et al*. 1993). However, this is only locally active in R6/2 mice (Davies *et al*. 1999; Turmaine *et al*. 2000). The increased Glu could also reflect its accumulation as an osmolyte at this stage in the disease process. Indeed, other osmolytes, such as Tau and *myo*-Ins, are also prominently elevated at 12 weeks.

Tau is elevated in the putamen of HD patients (Gramsbergen *et al*. 1986) and in the cortex and striatum of aged R6/2 mice (Jenkins *et al*. 2000, 2005). We also found a 36% elevation in taurine in 12, but not 8-week-old R6/2 mice. Tau has been assigned numerous functions in the CNS, including neuromodulator, neurotransmitter, osmolyte and neuroprotectant (Foos and Wu 2002). Appreciable amounts of Tau are released from astrocytes in response to hyposmolarity, hypoxia, ischemia, oxidative stress, and metabolic toxins (Reymond *et al*. 1996; Saransaari and Oja 2000; Foos and Wu 2002). Strikingly, the increased Tau, Gln, Glu, PCr, total Cr, GPC and *myo*-Ins and decreased Lac observed in R6/2 mice at 12 weeks resemble the pattern of changes in these metabolites observed by both analytical methods and *ex vivo* ^{1}H NMR spectroscopy following hypernatremia (Thurston *et al*. 1983; Heilig *et al*. 1989). Hypernatremia could result from insufficient energy to power the Na–K–ATPase to maintain intracellular ion concentrations or the reported decrease in Na–K–ATPase mRNA in R6/2 mice (Luthi-Carter *et al*. 2002).

The decrease in NAA concentration and subsequent increase in Tau concentration verify that conclusions reached in earlier HD studies, reporting signal ratios relative to tCr signal, indeed reflected decreases in NAA and increases in Tau (Jenkins *et al*. 2000, 2005).

However, the reported 50–60% decrease of NAA/tCr (Jenkins *et al*. 2000, 2005) is attributable to a 16–22% drop in NAA combined with a 27–31% increase in Cr + PCr demonstrated here. The decreased levels of NAA in R6/2 mice may reflect mitochondrial impairment (Bates *et al*. 1996), decreased neuronal integrity or neuronal dysfunction as consistently observed in neurological diseases (Demougeot *et al*. 2004).

The largest percent change in a metabolite was the increase in GPC at 12 weeks. Increases in GPC levels in cortical gray matter measured analytically from severely demented Alzheimers disease brains have been attributed to membrane breakdown (Nitsch *et al*. 1992). However, this same study did not find increases in GPC in human Huntington's disease cortical gray matter. Alternatively, elevated GPC levels could result from inactivation of its catabolism. GPC cholinephosphodiesterase, an enzyme that catalyzes conversion of GPC into glycerol and PCho, undergoes oxidative inactivation (Sok 1998). GPC cholinephosphodiesterase activity, selectively enriched in oligodendrocytes, was decreased in three different rodent models of demyelination (Yuan *et al*. 1992). Oxidative damage is characteristic of R6/2 brains (Tabrizi *et al*. 2000) and white matter damage occurs in HD (Ciarmiello *et al*. 2006). Thus, the possibility exists that the increase in GPC but not PCho in R6/2 striatum may reflect metabolic changes in white matter tracts that traverse this region.

The pattern of metabolite changes observed in the R6/2 mouse contrast with those observed in two other models of HD. The transgenic R6/2 mouse overexpresses an N-terminal fragment of human Huntingtin with 150 or more CAG repeats and is considered to model juvenile onset HD, the severest form of the disease. quinolinic acid-induced excitotoxicity has been proposed as a model of the final steps in the cell death pathway in HD (Beal *et al*. 1986). Chronic exposure to the complex II inhibitor, 3NP, has been used to mimic the metabolic insufficiency proposed to accompany HD (Brouillet *et al*. 1993). In normal rats and mice, basal levels of metabolites detectable by ^{1}H NMR spectrosocpy are comparable, making comparisons of these disease models plausible (Pfeuffer *et al*. 1999; Tkac *et al*. 2004). While NAA decreases in all three models, other metabolites do not change in similar manner. In both QA-treated rats and R6/2 mice at 8 weeks, Gln increased and Glu decreased. Other metabolite changes, however, are not similar. By 12 weeks in R6/2, Glu concentration increased. In R6/2, Tau, GSH and Cr + PCr increased, while in the QA-treated rats, these metabolites decreased (Tkac *et al*. 2001). Lac, GPC + PCho, *myo*-Ins, and PE remained unchanged in QA-treated rats despite changes in R6/2 (Tkac *et al*. 2001). Total Cr and choline-containing compounds also decreased in the striatum of the 3NP-treated baboon (Dautry *et al*. 1999). These comparisons suggest that acute, relatively synchronous excitotoxic cell death produces a metabolic pattern quite distinct from that observed in the transgenic animal where cell death, if present, will affect only a small proportion of neurons at any one time. The distinct metabolite profile of the R6/2 mouse indicated that if this is a faithful model of HD, the neurodegenerative mechanisms may be more complex than either TCA and electron transport impairment or excitotoxicty. Thus, the metabolic changes observed in R6/2 may reflect the ongoing balance between multiple processes: initial compensatory changes, secondary consequences, and in later stages, the denouement to cellular dysfunction and death.

Acknowledgments

We thank Dr Jean H. Thurston for insightful discussions and Dorothee Aeppli, Ph.D., Biostatistics Consulting Lab for statistical consultations. This work was supported by NIH F30-MH12157, NIH P41 RR08079, the Keck Foundation, the MIND Institute, the Biomedical Engineering Institute of the University of Minnesota and the Huntington's Disease Society of America.

Abbreviations used

Ala	alanine
Asc	ascorbate
Cho	choline-containing compounds
Cr	creatine
CRLB	Cramer-Rao lower bounds
FID	free induction decay
GABA	γ-aminobutyric acid
Glc	glucose
Gln	glutamine
Glu	glutamate
Glx	the sum of glutamine and glutamate
GPC	glycerophosphorylcholine
GSH	glutathione
HD	Huntington's disease
myo-Ins	*myo*-inositol
Lac	lactate
NAA	*N*-acetylaspartate
NAAG	*N*-acetylaspartylglutamate
NT	number of transients
PCho	phosphorylcholine
PCr	phosphocreatine
PE	phosphorylethanolamine
Tau	taurine
tCr	total creatine
TE	echo time
TR	repetition time
VOI	volume of interest
WT	wild type

References

Aylward EH, Sparks BF, Field KM, et al. Onset and rate of striatal atrophy in preclinical Huntington disease. Neurology 2004;63:66–72. [PubMed: 15249612]

Bates TE, Strangward M, Keelan J, Davey GP, Munro PM, Clark JB. Inhibition of *N*-acetylaspartate production: implications for 1H MRS studies *in vivo*. Neuroreport 1996;7:1397–1400. [PubMed: 8856684]

Beal MF. Mitochondria take center stage in aging and neuro-degeneration. Ann. Neurol 2005;58:495–505. [PubMed: 16178023]

Beal MF, Kowall NW, Ellison DW, Mazurek MF, Swartz KJ, Martin JB. Replication of the neurochemical characteristics of Huntington's disease by quinolinic acid. Nature 1986;321:168–171. [PubMed: 2422561]

Behrens PF, Franz P, Woodman B, Lindenberg KS, Landwehrmeyer GB. Impaired glutamate transport and glutamate-glutamine cycling: downstream effects of the Huntington mutation. Brain 2002;125:1908–1922. [PubMed: 12135980]

Benjamini Y, Hochberg Y. Controlling the false discovery rate: a practical and powerful approach to multiple testing. Roy. Stat. Soc. B 1995;1:289–300.

Bonavita S, Di Salle F, Tedeschi G. Proton MRS in neurological disorders. Eur. J. Radiol 1999;30:125–131. [PubMed: 10401593]

Brand A, Richter-Landsberg C, Leibfritz D. Multinuclear NMR studies on the energy metabolism of glial and neuronal cells. Dev. Neurosci 1993;15:289–298. [PubMed: 7805581]

Brouillet E, Jenkins BG, Hyman BT, Ferrante RJ, Kowall NW, Srivastava R, Roy DS, Rosen BR, Beal MF. Age-dependent vulnerability of the striatum to the mitochondrial toxin 3-nitropropionic acid. J. Neurochem 1993;60:356–359. [PubMed: 8417157]

Butterworth J, Yates CM, Reynolds GP. Distribution of phosphate-activated glutaminase, succinic dehydrogenase, pyruvate dehydrogenase and gamma-glutamyl transpeptidase in postmortem brain from Huntington's disease and agonal cases. J. Neurol. Sci 1985;67:161–171. [PubMed: 2858515]

Ciarmiello A, Cannella M, Lastoria S, Simonelli M, Frati L, Rubinsztein DC, Squitieri F. Brain white-matter volume loss and glucose hypometabolism precede the clinical symptoms of Huntington's disease. J. Nucl. Med 2006;47:215–222. [PubMed: 16455626]

Dautry C, Conde F, Brouillet E, Mittoux V, Beal MF, Bloch G, Hantraye P. Serial ^{1}H NMR spectroscopy study of metabolic impairment in primates chronically treated with the succinate dehydrogenase inhibitor 3-nitropropionic acid. Neurobiol. Dis 1999;6:259–268. [PubMed: 10448053]

Davies SW, Turmaine M, Cozens BA, Raza AS, Mahal A, Mangiarini L, Bates GP. From neuronal inclusions to neurodegeneration: neuropathological investigation of a transgenic mouse model of Huntington's disease. Philos. Trans. R. Soc. Lond. B Biol. Sci 1999;354:981–989.

van Dellen A, Welch J, Dixon RM, Cordery P, York D, Styles P, Blakemore C, Hannan AJ. *N*-Acetylaspartate and DARPP-32 levels decrease in the corpus striatum of Huntington's disease mice. Neuroreport 2000;11:3751–3757. [PubMed: 11117485]

Demougeot C, Marie C, Giroud M, Beley A. *N*-acetylaspartate: a literature review of animal research on brain ischaemia. J. Neurochem 2004;90:776–783. [PubMed: 15287882]

Dunlop DS, Mc Hale DM, Lajtha A. Decreased brain *N*-acetylaspartate in Huntington's disease. Brain Res 1992;580:44–48. [PubMed: 1387037]

Duyao M, Ambrose C, Myers R, Novelletto A, Persichetti F, Frontali M, Folstein S, Ross C, Franz M, Abbott M. Trinucleotide repeat length instability and age of onset in Huntington's disease. Nat. Genet 1993;4:387–392. [PubMed: 8401587]

Foos TM, Wu JY. The role of taurine in the central nervous system and the modulation of intracellular calcium homeostasis. Neurochem. Res 2002;27:21–26. [PubMed: 11926272]

Garseth M, Sonnewald U, White LR, Rod M, Zwart JA, Nygaard O, Aasly J. Proton magnetic resonance spectroscopy of cerebrospinal fluid in neurodegenerative disease: indication of glial energy impairment in Huntington chorea, but not Parkinson disease. J. Neurosci. Res 2000;60:779–782. [PubMed: 10861790]

Gramsbergen JB, Veenma-Van der Duin L, Venema K, Korf J. Cerebral cation shifts and amino acids in Huntington's disease. Arch. Neurol 1986;43:1276–1281. [PubMed: 2877650]

Gruetter R. Automatic, localized *in vivo* adjustment of all first- and second-order shim coils. Magn. Reson. Med 1993;29:804–811. [PubMed: 8350724]

Gruetter R, Tkac I. Field mapping without reference scan using asymmetric echo-planar techniques. Magn. Reson. Med 2000;43:319–323. [PubMed: 10680699]

Harms L, Meierkord H, Timm G, Pfeiffer L, Ludolph AC. Decreased *N*-acetyl-aspartate/choline ratio and increased lactate in the frontal lobe of patients with Huntington's disease: a proton magnetic resonance spectroscopy study. J. Neurol. Neurosurg. Psychiatry 1997;62:27–30. [PubMed: 9010396]

Heilig CW, Stromski ME, Blumenfeld JD, Lee JP, Gullans SR. Characterization of the major brain osmolytes that accumulate in salt-loaded rats. Am. J. Physiol 1989;257:F1108–F1116. [PubMed: 2603957]

Hoang TQ, Bluml S, Dubowitz DJ, Moats R, Kopyov O, Jacques D, Ross BD. Quantitative proton-decoupled 31P MRS and 1H MRS in the evaluation of Huntington's and Parkinson's diseases. Neurology 1998;50:1033–1040. [PubMed: 9566391]

Huntington G. On chorea. Adv. Neurol 1872;1:33–35.

Huntington's Disease Collaborative ResearchGroup. A novel gene containing a trinucleotide repeat that is expanded and unstable on Huntington's disease chromosomes. Cell 1993;72:971–983. [PubMed: 8458085]

Jenkins BG, Koroshetz WJ, Beal MF, Rosen BR. Evidence for impairment of energy metabolism *in vivo* in Huntington's disease using localized ^{1}H NMR spectroscopy. Neurology 1993;43:2689–2695. [PubMed: 8255479]

Jenkins BG, Rosas HD, Chen YC, Makabe T, Myers R, MacDonald M, Rosen BR, Beal MF, Koroshetz WJ. ^{1}H NMR spectroscopy studies of Huntington's disease: correlations with CAG repeat numbers. Neurology 1998;50:1357–1365. [PubMed: 9595987]

Jenkins BG, Klivenyi P, Kustermann E, Andreassen OA, Ferrante RJ, Rosen BR, Beal MF. Nonlinear decrease over time in *N*-acetyl aspartate levels in the absence of neuronal loss and increases in glutamine and glucose in transgenic Huntington's disease mice. J. Neurochem 2000;74:2108–2119. [PubMed: 10800956]

Jenkins BG, Andreassen OA, Dedeoglu A, Leavitt B, Hayden M, Borchelt D, Ross CA, Ferrante RJ, Beal MF. Effects of CAG repeat length, HTT protein length and protein context on cerebral metabolism measured using magnetic resonance spectroscopy in transgenic mouse models of Huntington's disease. J Neurochem 2005;95:553–562. [PubMed: 16135087]

Kasparova S, Sumbalova Z, Horecky J, Bystricky P, Mlynarik V, Gvozdjakova A, Liptaj T. New magnetic resonance spectroscopy biomarker for monitoring neurodegenerative diseases: animal models. Biomed. Pap. Med. Fac. Univ. Palacky Olomouc. Czech. Repub 2005;149:373–376. [PubMed: 16601791]

Klapstein GJ, Fisher RS, Zanjani H, Cepeda C, Jokel ES, Chesselet MF, Levine MS. Electrophysiological and morphological changes in striatal spiny neurons in R6/2 Huntington's disease transgenic mice. J Neurophysiol 2001;86:2667–2677. [PubMed: 11731527]

Koroshetz WJ, Jenkins BG, Rosen BR, Beal MF. Energy metabolism defects in Huntington's disease and effects of coenzyme Q10. Ann Neurol 1997;41:160–165. [PubMed: 9029064]

Landles C, Bates GP. Huntingtin and the molecular pathogenesis of Huntington's disease. Fourth in molecular medicine review series. EMBO Rep 2004;5:958–963. [PubMed: 15459747]

Levine MS, Cepeda C, Hickey MA, Fleming SM, Chesselet MF. Genetic mouse models of Huntington's and Parkinson's diseases: illuminating but imperfect. Trends Neurosci 2004;27:691–697. [PubMed: 15474170]

Li SH, Li XJ. Huntingtin and its role in neuronal degeneration. Neuroscientist 2004;10:467–475. [PubMed: 15359012]

Lievens JC, Woodman B, Mahal A, Spasic-Boscovic O, Samuel D, Kerkerian-Le Goff L, Bates GP. Impaired glutamate uptake in the R6 Huntington's disease transgenic mice. Neurobiol Dis 2001;8:807–821. [PubMed: 11592850]

Lodi R, Schapira AH, Manners D, Styles P, Wood NW, Taylor DJ, Warner TT. Abnormal *in vivo* skeletal muscle energy metabolism in Huntington's disease and dentatorubropallidoluysian atrophy. Ann. Neurol 2000;48:72–76. [PubMed: 10894218]

Luthi-Carter R, Hanson SA, Strand AD, Bergstrom DA, Chun W, Peters NL, Woods AM, Chan EY, Kooperberg C, Krainc D, Young AB, Tapscott SJ, Olson JM. Dysregulation of gene expression in the R6/2 model of polyglutamine disease: parallel changes in muscle and brain. Hum Mol Genet 2002;11:1911–1926. [PubMed: 12165554]

Mangiarini L, Sathasivam K, Seller M, Cozens B, Harper A, Hetherington C, Lawton M, Trottier Y, Lehrach H, Davies SW, Bates GP. Exon 1 of the HD gene with an expanded CAG repeat is sufficient to cause a progressive neurological phenotype in transgenic mice. Cell 1996;87:493–506. [PubMed: 8898202]

Milakovic T, Johnson GV. Mitochondrial respiration and ATP production are significantly impaired in striatal cells expressing mutant huntingtin. J Biol Chem 2005;280:30773–30782. [PubMed: 15983033]

Nance MA. Huntington disease: clinical, genetic, and social aspects. J. Geriatr. Psychiatry Neurol 1998;11:61–70. [PubMed: 9877527]

Nicoli F, Vion-Dury J, Maloteaux JM, Delwaide C, Confort-Gouny S, Sciaky M, Cozzone PJ. CSF and serum metabolic profile of patients with Huntington's chorea: a study by high resolution proton NMR spectroscopy and HPLC. Neurosci. Lett 1993;154:47–51. [PubMed: 8361646]

Nitsch RM, Blusztajn JK, Pittas AG, Slack BE, Growdon JH, Wurtman RJ. Evidence for a membrane defect in Alzheimer disease brain. Proc. Natl Acad. Sci. USA 1992;89:1671–1675. [PubMed: 1311847]

Norenberg MD, Martinez-Hernandez A. Fine structural localization of glutamine synthetase in astrocytes of rat brain. Brain Res 1979;161:303–310. [PubMed: 31966]

Oz G, Tkac I, Charnas LR, Choi IY, Bjoraker KJ, Shapiro EG, Gruetter R. Assessment of adrenoleukodystrophy lesions by high field MRS in non-sedated pediatric patients. Neurology 2005;64:434–441. [PubMed: 15699371]

Pfeuffer J, Tkac I, Provencher SW, Gruetter R. Toward an *in vivo* neurochemical profile: quantification of 18 metabolites in short-echo-time (1)H NMR spectra of the rat brain. J. Magn. Reson 1999;141:104–120. [PubMed: 10527748]

Provencher SW. Estimation of metabolite concentrations from localized *in vivo* proton NMR spectra. Magn. Reson. Med 1993;30:672–679. [PubMed: 8139448]

Puranam KL, Wu G, Strittmatter WJ, Burke JR. Polyglutamine expansion inhibits respiration by increasing reactive oxygen species in isolated mitochondria. Biochem. Biophys. Res. Commun 2006;341:607–613. [PubMed: 16427603]

Raman L, Tkac I, Ennis K, Georgieff MK, Gruetter R, Rao R. *In vivo* effect of chronic hypoxia on the neurochemical profile of the developing rat hippocampus. Brain Res. Dev. Brain Res 2005;156:202–209.

Reymond I, Almarghini K, Tappaz M. Immunocytochemical localization of cysteine sulfinate decarboxylase in astrocytes in the cerebellum and hippocampus: a quantitative double immunofluorescence study with glial fibrillary acidic protein and S-100 protein. Neuroscience 1996;75:619–633. [PubMed: 8931024]

Rosenblatt A, Abbott MH, Gourley LM, Troncoso JC, Margolis RL, Brandt J, Ross CA. Predictors of neuropatho-logical severity in 100 patients with Huntington's disease. Ann. Neurol 2003;54:488–493. [PubMed: 14520661]

Sanchez-Pernaute R, Garcia-Segura JM, del Barrio Alba A, Viano J, de Yebenes JG. Clinical correlation of striatal 1H MRS changes in Huntington's disease. Neurology 1999;53:806–812. [PubMed: 10489045]

Saransaari P, Oja SS. Taurine and neural cell damage. Amino Acids 2000;19:509–526. [PubMed: 11140356]

Sawa A, Wiegand GW, Cooper J, Margolis RL, Sharp AH, Lawler JF Jr. Greenamyre JT, Snyder SH, Ross CA. Increased apoptosis of Huntington disease lymphoblasts associated with repeat length-dependent mitochondrial depolarization. Nature Med 1999;5:1194–1198. [PubMed: 10502825]

Seong IS, Ivanova E, Lee JM, et al. HD CAG repeat implicates a dominant property of huntingtin in mitochondrial energy metabolism. Hum. Mol. Genet 2005;14:2871–2880. [PubMed: 16115812]

Sok DE. Ascorbate-induced oxidative inactivation of Zn^{2+}-glycerophosphocholine cholinephosphodiesterase. J. Neurochem 1998;70:1167–1174. [PubMed: 9489738]

Tabrizi SJ, Workman J, Hart PE, Mangiarini L, Mahal A, Bates G, Cooper JM, Schapira AHV. Mitochondrial dysfunction and free radical damage in the Huntington R6/2 transgenic mouse. Ann. Neurol 2000;47:80–86. [PubMed: 10632104]

Taylor-Robinson SD, Weeks RA, Bryant DJ, Sargentoni J, Marcus CD, Harding AE, Brooks DJ. Proton magnetic resonance spectroscopy in Huntington's disease: evidence in favour of the glutamate excitotoxic theory. Mov. Disord 1996;11:167–173. [PubMed: 8684387]

Thurston JH, Hauhart RE, Dirgo JA, McDougal DB Jr. Insulin and brain metabolism. Absence of direct action of insulin on K^+ and Na^+ transport in normal rabbit brain. Diabetes 1977;26:1117–1119. [PubMed: 590636]

Thurston JH, Hauhart RE, Schulz DW. Effect of chronic hypernatremic dehydration and rapid rehydration on brain carbohydrate, energy, and amino acid metabolism in weanling mice. J. Neurochem 1983;40:240–245. [PubMed: 6848662]

Tkac I, Starcuk Z, Choi IY, Gruetter R. *In vivo* ^{1}H NMR spectroscopy of rat brain at 1 ms echo time. Magn. Reson. Med 1999;41:649–656. [PubMed: 10332839]

Tkac I, Keene CD, Pfeuffer J, Low WC, Gruetter R. Metabolic changes in quinolinic acid-lesioned rat striatum detected non-invasively by *in vivo* (1)H NMR spectroscopy. J. Neurosci. Res 2001;66:891–898. [PubMed: 11746416]

Tkac I, Rao R, Georgieff MK, Gruetter R. Developmental and regional changes in the neurochemical profile of the rat brain determined by in vivo 1H NMR spectroscopy. Magn. Reson. Med 2003;50:24–32. [PubMed: 12815675]

Tkac I, Henry PG, Andersen P, Keene CD, Low WC, Gruetter R. Highly resolved *in vivo* ^{1}H NMR spectroscopy of the mouse brain at 9.4 T. Magn. Reson. Med 2004;52:478–484. [PubMed: 15334565]

Tsang TM, Woodman B, McLoughlin GA, Griffin JL, Tabrizi SJ, Bates GP, Holmes E. Metabolic characterization of the R6/2 transgenic mouse model of Huntington's disease by high-resolution MAS ^{1}H NMR spectroscopy. J. Proteome. Res 2006;5:483–492. [PubMed: 16512662]

Turmaine M, Raza A, Mahal A, Mangiarini L, Bates GP, Davies SW. Nonapoptotic neurodegeneration in a transgenic mouse model of Huntington's disease. Proc. Natl Acad. Sci. USA 2000;97:8093–8097. [PubMed: 10869421]

Vonsattel JP, Myers RH, Stevens TJ, Ferrante RJ, Bird ED, Richardson EP Jr. Neuropathological classification of Huntington's disease. J. Neuropathol. Exp. Neurol 1985;44:559–577. [PubMed: 2932539]

Wang X, Sarkar A, Cicchetti F, Yu M, Zhu A, Jokivarsi K, Saint-Pierre M, Brownell AL. Cerebral PET imaging and histological evidence of transglutaminase inhibitor cystamine induced neuroprotection in transgenic R6/2 mouse model of Huntington's disease. J Neurol Sci 2005;231:57–66. [PubMed: 15792822]

Yuan J, McCartney DG, Monge M, Espinosa de Los MA, Zalc B, de Vellis J, Kanfer JN. Glycerophosphorylcholine phosphocholine phosphodiesterase activity in cultured oligodendrocytes, astrocytes, and central nervous tissue of dysmyelinating rodent mutants. J. Neurosci. Res 1992;31:68–74. [PubMed: 1319506]

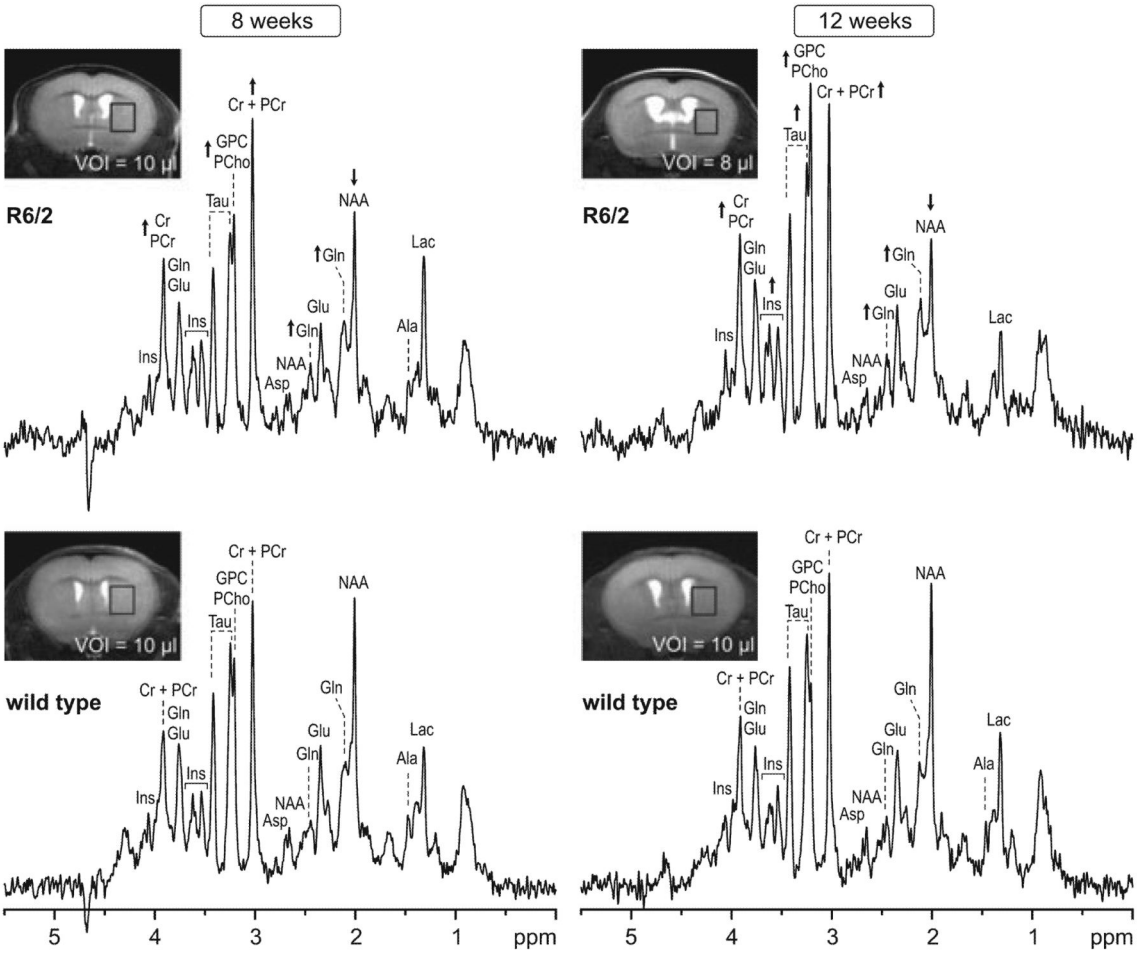

Fig. 1.

Representative *in vivo* ^{1}H NMR spectra measured from striata of Huntington's disease transgenic R6/2 and wild type mice at 8 and 12 weeks of age. Insets: MR images with the selected volume of interest centered rostrocaudally at the level of the anterior commissure. Arrows indicate changes of a specific metabolite in R6/2 mice relative to age matched WT control. STEAM, TE = 2 ms, TR = 5 s, NT = 160. Processing: Gaussian multiplication (σ = 0.085 s), FT and zero-order phase correction. No water signal removal or baseline correction was applied.

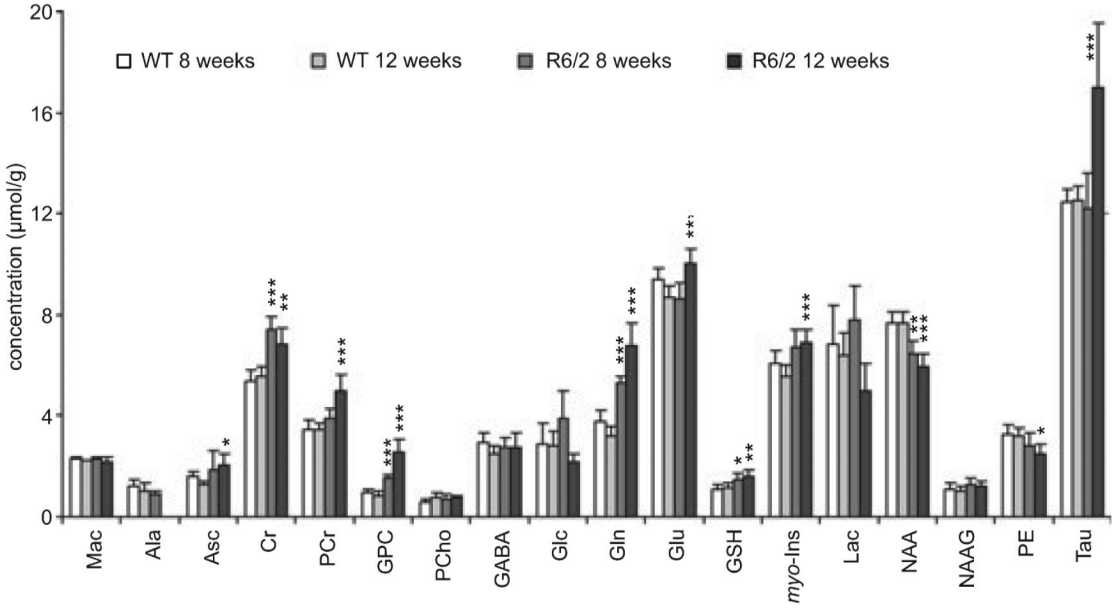

Fig. 2.

Metabolite concentrations quantified from striata of wild type and R6/2 mice at 8 and 12 weeks of age. Statistically significant differences are noted for comparisons between metabolite concentrations of R6/2 and wild type mice at each age. For comparisons between ages within each strain, see Table 1. Data represent mean ± SD, $n = 6–9$. Significance level: $*p < 0.01$, $**p < 0.002$, $***p < 0.0002$.

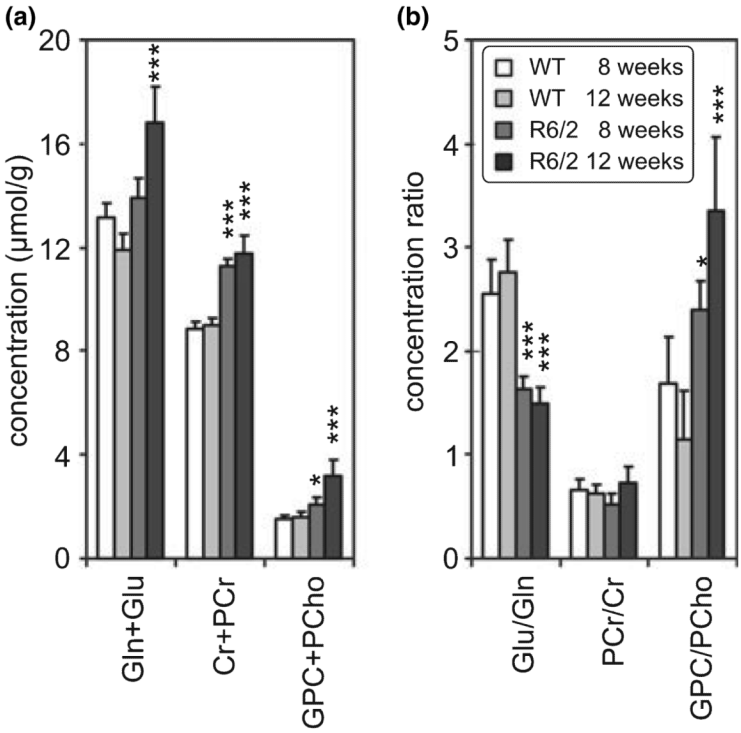

Fig. 3.

Summed concentrations (a) and concentration ratios (b) of selected pairs of metabolites (Gln and Glu, PCr and Cr, GPC and PCho) that are difficult to resolve at lower magnetic field strengths (mean ± SD). Metabolites quantified from striata of R6/2 and wild type mice at 8 and 12 weeks of age. Statistically significant differences are shown for comparisons between R6/2 and wild type mice at each age. Significance level: *$p < 0.05$, **$p < 0.01$, ***$p < 0.001$. Additionally, significant differences between 8 and 12-week-old R6/2 mice were found for Gln + Glu ($p < 0.001$), GPC + PCho ($p < 0.001$), PCr/Cr ($p < 0.01$) and GPC/PCho ($p < 0.001$).

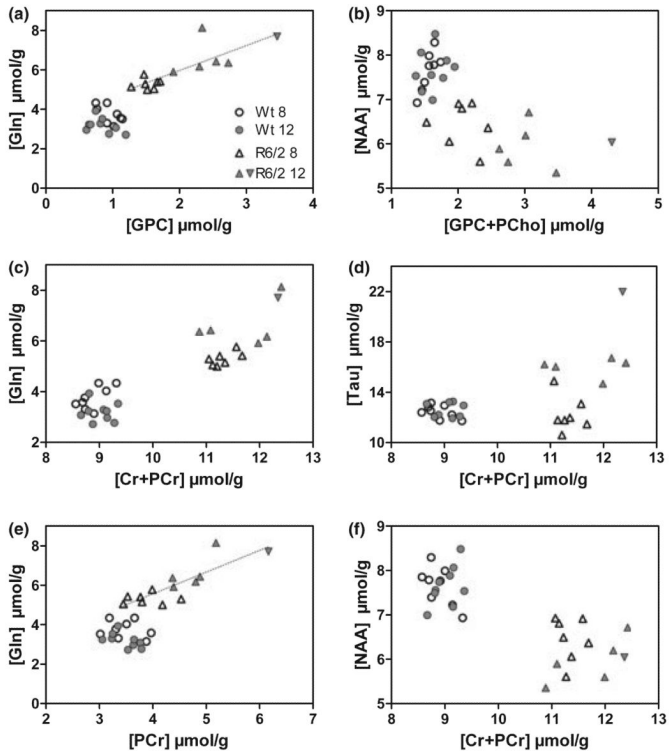

Fig. 4.

Scatter plots of selected metabolite concentrations quantified from individual mice distinguished between R6/2 and wild type at 8 and 12 weeks of age. For the R6/2 data, dotted lines represent correlation between Gln and GPC (a; $r = 0.81$, $p = 0.0008$), Gln and PCr (e; $r = 0.84$, $p = 0.0003$), Gln and Tau (not shown, $r = 0.82$, $p = 0.0006$). To illustrate the ability to track individual animals, values from one particular R6/2 mouse are highlighted with an inverted, filled triangle.

Table 1

Relative changes in striatal metabolite concentrations between WT and R6/2 mice at 8 and 12 weeks of age and between different ages of the same strain

	% Change in R6/2 relative to WT		% Change at 12 weeks relative to 8 weeks	
Metabolite	**At 8 weeks**	**At 12 weeks**	**WT**	**R6/2**
Mac	1	−2	−3	−6
Ala	−25		−15	
Asc	16	62*	−21	10
Cr	38***	23**	3	−8
PCr	12	43***	0	28*
GPC	60***	206***	−13	66**
PCho	19	−3	33	8
GABA	−7	10	−15	0
Glc	33	−23	−2	−44*
Gln	41***	113***	−15	28**
Glu	−9	16**	−8	17**
GSH	36*	39**	8	10
myo-Ins	11	25***	−8	3
Lac	14	−23	−6	−36*
NAA	−16**	−22***	0	−8
NAAG	16	13	−6	−8
PE	−15	−22*	−3	−11
Tau	−2	36***	1	39**

Statistical comparisons were made using absolute metabolite concentrations (Fig. 2) and are repeated here for convenience. Significance level:

* $p < 0.01$

** $p < 0.002$

*** $p < 0.0002$.